Transition of dominant deformation mode in bulk polycrystalline pure Mg by ultra-grain refinement down to sub-micrometer

AUTHOR(S):

Zheng, Ruixiao; Du, Jun-Ping; Gao, Si; Somekawa, Hidetoshi; Ogata, Shigenobu; Tsuji, Nobuhiro

CITATION:

Zheng, Ruixiao ...[et al]. Transition of dominant deformation mode in bulk polycrystalline pure Mg by ultra-grain refinement down to sub-micrometer. Acta Materialia 2020, 198: 35-46

ISSUE DATE:

2020-10

URL:

http://hdl.handle.net/2433/255222

Acta Materialia 198 (2020) 35–46

Contents lists available at ScienceDirect

Acta Materialia

journal homepage: www.elsevier.com/locate/actamat

Full length article

Transition of dominant deformation mode in bulk polycrystalline pure Mg by ultra-grain refinement down to sub-micrometer

Ruixiao Zheng[a,b,*], Jun-Ping Du[c,d], Si Gao[b], Hidetoshi Somekawa[e], Shigenobu Ogata[d,c,*], Nobuhiro Tsuji[b,c,*]

[a] School of Materials Science and Engineering, Beihang University, Beijing 100191, China
[b] Department of Materials Science and Engineering, Kyoto University, Yoshida Honmachi, Sakyo-ku, Kyoto 606-8501, Japan
[c] Elements Strategy Initiative for Structural Materials (ESISM), Kyoto University, Yoshida Honmachi, Sakyo-ku, Kyoto 606-8501, Japan
[d] Department of Mechanical Science and Bioengineering, Osaka University, Osaka 560-8531, Japan
[e] Research Center for Structural Materials, National Institute for Materials Science, 1-2-1 Sengen, Tsukuba 305-0047, Japan

ARTICLE INFO

Article history:
Received 11 April 2020
Revised 16 June 2020
Accepted 24 July 2020
Available online 28 July 2020

Keywords:
Magnesium
Strength and ductility
Deformation mode
Hall-petch relationship
Grain size

ABSTRACT

Magnesium (Mg) and its alloys usually show relatively low strength and poor ductility at room temperature due to their anisotropic hexagonal close-packed (HCP) crystal structure that provides a limited number of independent slip systems. Here we report that unique combinations of strength and ductility can be realized in bulk polycrystalline pure Mg by tuning the predominant deformation mode. We succeeded in obtaining the fully recrystallized specimens of pure Mg having a wide range of average grain sizes, of which minimum grain size was 650 nm, and clarified mechanical properties and deformation mechanisms at room temperature systematically as a function of the grain size. Deformation twinning and basal slip governed plastic deformation in the conventional coarse-grained region, but twinning was suppressed when the grain size was refined down to several micro-meters. Eventually, grain boundary mediated plasticity, *i.e.*, grain boundary sliding became dominant in the ultrafine-grained (UFG) specimen having a mean grain size smaller than 1 μm. The transition of the deformation modes led to a significant increase of tensile elongation and breakdown of Hall-Petch relationship. It was quantitatively confirmed by detailed microstructural observation and theoretical calculation that the change in strength and ductility arose from the distinct grain size dependence of the critical shear stress for activating different deformation modes.

1. Introduction

As the lightest structural metal with a density ~ 1.74 g/cm^3, Mg and its alloys are increasingly used as structural components in automotive and aerospace industries for reducing weights and increasing fuel efficiency [1-3]. On the other hand, Mg suffers from relatively low strength, limited ductility and poor cold workability compared with other widely used metals such as iron and aluminum. Mg has a hexagonal close-packed (HCP) crystal structure possessing only one close packed plane (basal plane), resulting in a highly anisotropy in critical resolved shear stress (CRSS) for different slip systems [4, 5]. It has been reported that the CRSS values at ambient temperature for non-basal slip systems (prismatic and/or pyramidal) were two orders of magnitude higher than that for a basal slip system in single crystal of Mg [6]. Such an extreme plastic anisotropy in CRSS makes non-basal slips very difficult to be activated. However, basal slip system itself fails to satisfy the von-Mises criterion that requires five independent slip systems for successful plastic deformation in polycrystals, resulting in poor cold workability as well as pronounced mechanical anisotropy in Mg. Deformation twinning is another important deformation mode that can provide deformation components along c-axis of HCP, competing against dislocation slips in Mg. The {10–12} extension twinning is readily activated in Mg and Mg alloys due to its relatively lower CRSS compared to non-basal slip and other twinning systems [7, 8]. Moreover, it has been reported that grain boundary-mediated plasticity, such as grain boundary sliding (GBS) and grain rotation,

* Corresponding authors.
E-mail addresses: zhengruixiao@buaa.edu.cn (R. Zheng), ogata@me.es.osaka-u.ac.jp (S. Ogata), nobuhiro-tsuji@mtl.kyoto-u.ac.jp (N. Tsuji).

https://doi.org/10.1016/j.actamat.2020.07.055

may also contribute to the plastic deformation in fine-grained Mg alloys, even at relatively low temperatures [9, 10].

We considered that there should be some internal parameters (such as grain size) and external parameters (such as temperature and strain rate) that can regulate the activity of various deformation modes, and thus control global mechanical properties of polycrystalline Mg [11]. A survey of recent literatures has demonstrated that it is possible to control the dominant deformation mode in metals with HCP structure by changing the average grain size (d) or crystal size [12-19]. For instance, Yu et al. [12] reported a strong crystal size effect on deformation twinning in a Ti-5at.%Al single crystal under micro- or nano-compression test. They found that the stress required for deformation twinning increased drastically with decreasing the sample (crystal) size down to 1 μm, below which deformation twinning was entirely replaced by dislocation slips. Yu et al. [13] also carried out *in situ* tensile tests in TEM using Mg single crystals having various sample sizes. Their results suggested that, in addition to the typical "the smaller, the stronger" tendency, the samples with extremely small sizes (gage cross section ~ 100 nm × 100 nm) exhibited a dramatically larger plastic strain before failure, which was believed to be due to the reduced anisotropy in CRSS among various slip systems. As a result, unusual slip systems having $\langle \boldsymbol{c} \rangle$ component in Burgers vector were significantly activated, leading to large ductility. It is important to note that grain boundary is absent in such single crystal specimens. For polycrystalline specimens, especially those having ultrafine-grained (UFG, d<1 μm) and nano-crystalline (NC, d<100 nm) microstructures, however, the situation might be different, because of the greatly increased fraction of grain boundaries.

Bulk UFG Mg alloys have been successfully fabricated by various kinds of severe plastic deformation methods, such as multiaxial forging process and alternate biaxial reverse corrugation process, and significantly enhanced mechanical properties were realized [14, 16]. However, the ultra-grain refinement of recrystallized pure Mg down to sub-micrometer scale is still challenging, due to pronounced recovery, recrystallization, and grain growth during processing at elevated temperatures. Recently, Zeng et al. [17] have refined the grain size of polycrystalline pure Mg down to 1.3 μm by means of warm extrusion. In contrast to the ultra-high strength obtained in the nanoscale single crystal of pure Mg, the compressive yield strength of the bulk fine-grained pure Mg was just slightly higher than that of the coarse-grained counterpart at a strain rate of 10^{-3} s^{-1}. On the other hand, the fine-grained pure Mg became super-formable at room temperature, namely, could be deformed to a compressive strain of 85% without failure. The authors claimed that the inter-granular deformation mechanisms became dominant when the grain size was reduced to the vicinity of 1 μm, rather than the usual dislocation slip and deformation twinning in conventional coarse-grained specimens. Somekawa et al. [18] also found that the role of GBS became significant in plastic deformation of a fine-grained pure Mg (d = 1.2 μm) at a very low tensile strain rate of 10^{-5} s^{-1}, which led to an exceptional large room temperature tensile elongation of 230% and a breakdown of the Hall-Petch relationship. However, such a transition of deformation modes has not yet been proved by systematic experiments using materials having various ultrafine grain sizes, and the critical grain size as well as the underlying mechanisms that change the dominant deformation mode in pure Mg have not been explored. Choi et al. [19] have investigated deformation behavior of UFG and NC pure Mg produced by powder metallurgy under a compression test with an initial strain rate 10^{-4} s^{-1} at room temperature. Their results suggested that UFG pure Mg (d = 400 nm) still exhibited strong work-hardening after yielding, while the role of GBS became significant when the grain size was reduced to 60 nm. The results obtained by Choi et al. was clearly different from those reported by Zeng et al. [17] and Somekawa et al. [18], especially about the critical grain size for changing the dominant deformation mode. It is considered that the much smaller grain size for realizing GBS in pure Mg processed by powder metallurgy was probably caused by contamination (like oxygen) introduced during mechanical milling, which may segregate along grain boundaries to inhibit GBS.

To the best of our knowledge, systematic experiments on the effect of grain size (from several tens of micrometers to sub-micrometer scale) on the change of deformation behavior at ambient temperature in contamination free bulk polycrystalline pure Mg have not been carried out. One of the main challenges is the poor formability of Mg, which makes it very difficult to apply large plastic strain to Mg in grain refinement processes without cracking [20]. Additionally, the melting temperature of Mg is low (650 °C). As a result, controlling grain sizes in Mg through annealing heat treatments is much restricted compared with other metals. However, we have recently succeeded in refining the average grain size of a commercial Mg alloy (ZKX600: Mg-6.2%Zn-0.5%Zr-0.2%Ca, mass%) down to 100 nm by means of severe plastic deformation using high pressure torsion (HPT) [21]. Furthermore, fully recrystallized microstructures with average grain sizes ranging from 0.77 μm to 23.3 μm could be prepared in the alloy through subsequent rapid annealing treatment after HPT. Although the minimum grain size obtained in pure Mg should be larger than that in Mg alloys due to enhanced recovery, recrystallization or/and grain growth, our preliminary results and previous literatures [22, 23] demonstrated a possibility to refine the grain size of pure Mg down to a sub-micrometer scale.

The aim of the present study is to systematically investigate the effect of grain size on the deformation behavior of bulk contamination-free pure Mg. We first tried to prepare specimens with a wide range of mean grain sizes by HPT and subsequent annealing treatment. We then carried out comprehensive mechanical property testing using a uniaxial tensile test and carefully observed tensile-deformed microstructures of the specimens. We have found in the current study that the yield strength, tensile elongation and the Hall-Petch relationship at room temperature are strongly affected by the grain size, which are associated with the change of dominant deformation modes. Underlying mechanisms is theoretically discussed based on the grain size dependence of CRSS for various deformation modes.

2. Experimental procedure

A commercial pure Mg with a purity of 99.9 mass% was used in this study. Disc-shaped specimens with a diameter of 10 mm and a thickness of 0.80 mm were sliced from a pure Mg ingot and provided for the HPT process. The HPT was performed at a rotation speed of 0.2 rpm under a compressive pressure of 6 GPa at room temperature. The total rotation angle applied in HPT was 1800° (5 rotations). After HPT, the specimens were annealed at various temperatures ranging from 100 °C to 450 °C for different periods of time. For the annealing heat treatments, an oil bath or a salt bath was used below or above 300 °C, respectively. The specimens were carefully wrapped by aluminum foil in annealing, in order to avoid oxidation of the specimens in annealing.

Microstructures of the specimens under various processing conditions were characterized by field emission type scanning electron microscopy (FE-SEM) using JSM-7100F equipped with an electron backscattering diffraction (EBSD) system. The SEM was operated at an accelerating voltage of 15 kV. Average grain sizes were measured by linear interception method on obtained EBSD inverse pole figure (IPF) and grain boundary (GB) maps. Microstructures of UFG specimens and dislocation structures after tensile deformation were also observed by transmission electron microscopy (TEM) using JEM-2010 operated at 200 kV. For the EBSD and TEM observations, areas at a distance of 3.0 mm from the center of the HPT

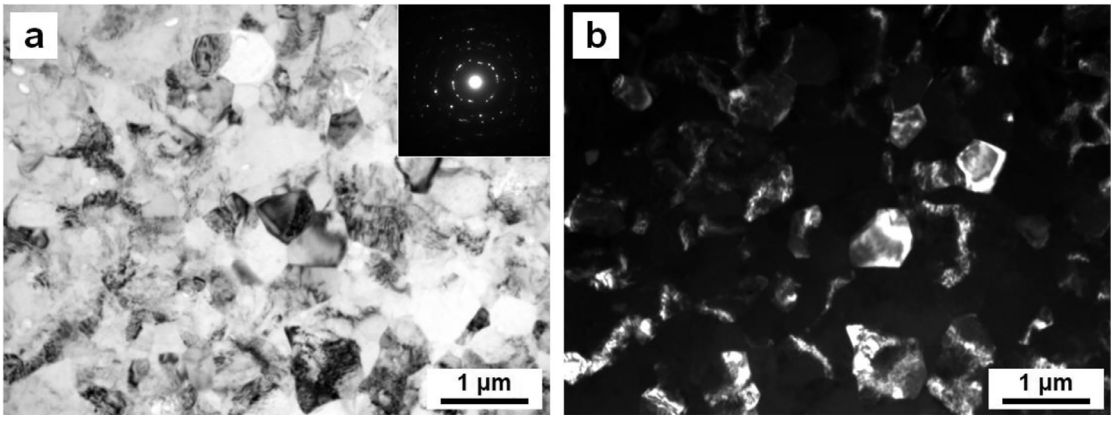

Fig. 1. TEM micrographs of the as-HPT processed specimen (d = 0.50 μm). (a) Bright field TEM image showing a mixture of equiaxed and dislocation-free recrystallized grains and grains including profuse dislocations. Selected area electron diffraction (SAD) pattern is inserted. (b) Corresponding dark field TEM image.

discs were mainly observed. Detailed preparation method of the EBSD and TEM specimens can be found in our previous publications [21].

Occurrence of GBS was also checked. Polished tensile specimens were placed in a focused ion beam (FIB) machine, and line patterns were drawn by focused Ga ion beam at an accelerated voltage of 30 kV and a current of 10 pA. The targeted dimensions of the lines were 100 μm in length, 0.1 μm in width and 0.1 μm in depth. Identical areas including the line markers on the tensile specimens were observed by SEM before and after the tensile deformation to various plastic strains.

Mechanical properties of the specimens with various grain sizes were characterized by an uniaxial tensile test at room temperature. Small-sized tensile specimens with a gage length of 2 mm and a gage cross section of 1 mm × 0.5 mm were cut from the HPT processed discs so that the center of the gage part matched with a radial distance of 3.0 mm from the center of the discs. The tensile direction was perpendicular to the radial direction. It has been confirmed in our previous studies [24] that the small-sized specimen can give reliable data equivalent to those obtained from standard-sized specimens of the same materials. Tensile tests were carried out at a quasi-static strain rate of 8.3×10^{-4} s^{-1}. The displacement of the gage section was precisely measured by a CCD video camera extensometer and the tensile strain was calculated by a digital image correlation (DIC) technique using a Vic-2D software. For each processing condition, at least three tensile specimens were tested, and the results showed good reproducibility.

3. Results

3.1. Microstructures of the hpt and annealed specimens

Fig. 1 shows TEM bright field (BF) and corresponding dark field (DF) images of the specimen HPT processed by 1800° rotation (5 rotations) at RT. The microstructure was covered by nearly equiaxed grains and the mean grain size was about 0.5 μm. Retained dislocation structures were observed within most of the grains, while some fully recrystallized grains formed dynamically during HPT were also found. The ring-like selected area diffraction (SAD) pattern inserted in Fig. 1(a) indicated that the UFGs had various orientations. These microstructural characteristics were consistent with the previous report by Edalati et al. [22], in which a partially recrystallized microstructure was obtained in a commercial pure Mg after HPT by 10 rotations (3600°) at RT.

The HPT processed specimen was subjected to subsequent annealing treatments for recrystallization. Fully recrystallized specimens with various mean grain sizes ranging from 0.65 μm to 59.7 μm were obtained by changing the annealing temperature and holding time. EBSD maps of several representative specimens are presented in Fig. 2. Both IPF maps (upper row) and corresponding GB maps (lower row) are displayed. All the specimens showed rather homogeneous microstructures without orientation (color) gradation inside grains, and the grains were surrounded mostly by high angle grain boundaries (HAGBs), indicating that these specimens were fully recrystallized. The average grain sizes (d) of the specimens shown in Fig. 2 were 0.65 μm, 2.46 μm, 7.27 μm and 59.7 μm, respectively. The microstructure of the UFG specimen (d = 0.65 μm) was also observed by TEM. The clean and equiaxed grains in the BF- and corresponding DF-TEM images displayed in Fig. 3 again confirmed recrystallized nature of the microstructure. As far as we know, the average grain size of 0.65 μm fabricated in the current study is the finest recrystallized grain size that has been obtained in bulk commercial purity Mg [22, 23]. A few {10–12} extension twins could be observed in the specimens having relatively coarse grain sizes (*e.g.* d = 7.27 μm in Fig. 2(e)), which might be introduced during mechanical polishing before observations. (0001) and (10–10) pole figures of the specimens shown in Fig. 2 are presented in Fig. S1 in the *supplementary material*. All the specimens showed typical basal recrystallization texture with their basal planes nearly parallel to the disk planes, *i.e.*, shear planes in the HPT deformation, which agreed with the colors in the EBSD IPF maps shown in Fig. 2 (a, c, e. g).

3.2. Tensile properties of the specimens having various grain sizes

Fully recrystallized pure Mg specimens with various mean grain sizes were provided for the uniaxial tensile tests at RT and obtained nominal stress-strain curves are shown in Fig. 4. Because the recrystallized specimens had similar texture (as was shown in Fig.S1), the change of the stress-strain behavior is mostly attributed to the different grain sizes. The specimen with a mean grain size of 59.7 μm exhibited a very low yield strength (YS: 0.2% proof stress) of 50 MPa, strong strain-hardening after yielding, and limited tensile ductility (total elongation ~0.10 (10%)). This is a typical mechanical behavior of pure Mg having conventional coarse-grained microstructures. With decreasing the grain size, the yield strength increased to a maximum value of 172 MPa at a grain size of 1.57 μm. The total elongation increased with the grain refinement, reached 0.25 (25%) at a grain size of 4.32 μm and then kept almost constant value (0.25~0.27) when the grain size became larger than 1.57 μm. It is noteworthy that a clear yield drop could be found at the beginning of plastic deformation in the specimens having mean grain sizes of 2.46 μm and 1.57 μm. This corresponded to the discontinuous yielding phenomena accompa-

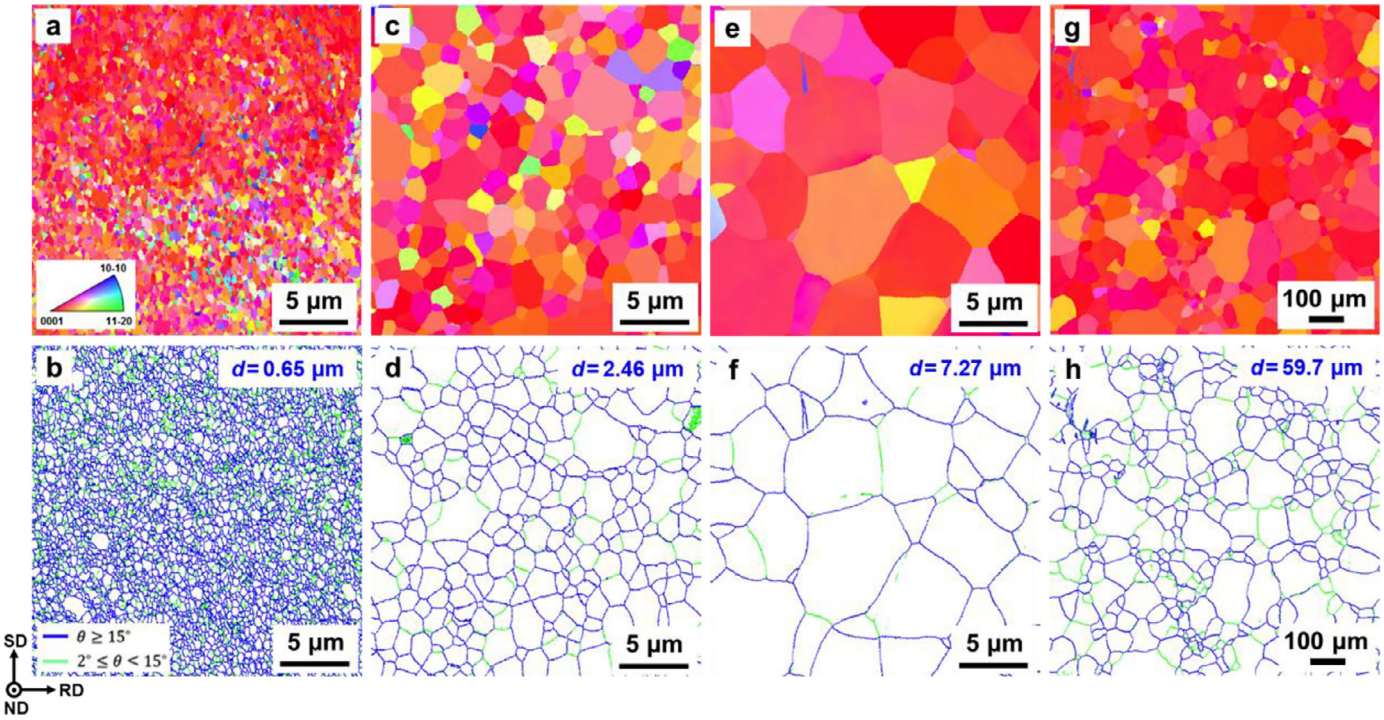

Fig. 2. EBSD IPF (upper row) and GB (lower row) maps of several representative specimens showing fully recrystallized microstructures with different mean grain sizes. (**a, b**) UFG specimen with a mean grain size of 0.65 μm (HPT by 1800° + annealing at 100 °C for 1 min). (**c, d**) Fine-grained specimen with a mean grain size of 2.46 μm (HPT by 1800° + annealing at 250 °C for 1 min). (**e, f**) Coarse-grained specimen with a mean grain size of 7.27 μm (HPT by 1800° + annealing at 300 °C for 60 min). (**g, h**) Coarse-grained specimen with a mean grain size of 59.7 μm (HPT by 1800° + annealing at 450 °C for 60 min). The colors in the IPF maps indicate crystallographic orientations parallel to the normal direction of the disk. The blue and green lines in the GB maps correspond to high angle grain boundaries (HAGBs) having misorientations larger than 15° and low angle grain boundaries (LAGBs) with misorientations between 2° and 15°, respectively.

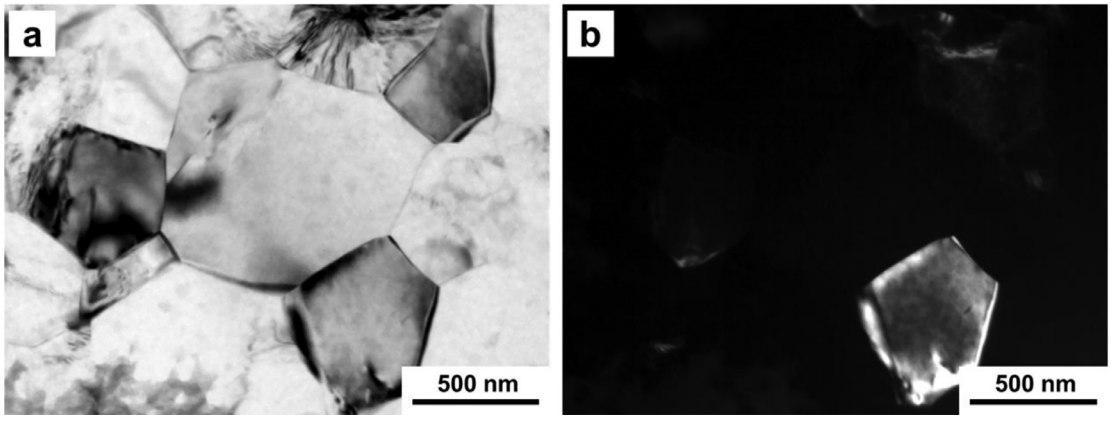

Fig. 3. TEM micrographs of the fully recrystallized UFG specimen (d = 0.65 μm). (**a**) BF-TEM image showing clean and equiaxed grains. (**b**) Corresponding DF-TEM image.

nying Lüders deformation that have been universally observed in other fully recrystallized ultrafine grained metallic materials [25, 26]. It is considered that the yield drop phenomena are due to the lack of mobile dislocations within very fine and recrystallized grains [27–29]. When the grain size was refined to 1.21 μm, the yield drop phenomena disappeared, and an obvious decrease in the yield strength was observed (YS = 141 MPa). The disappearance of the yield drop and the decrease of the yield strength suggest a change of deformation mechanisms. When the grain size furthermore decreased down to sub-micrometer (d = 0.65 μm), the deformation behavior totally changed. The specimen yielded at a very low stress of 87 MPa, which was just half of the YS (172 MPa) obtained in the fine-grained specimen (d = 1.57 μm). Upon yielding, the specimen underwent work hardening and reached an ultimate tensile strength of 135 MPa at a nominal strain of 0.09. After that, the nominal flow stress decreased gradually with further increasing the nominal strain, and showed a pretty large total elongation of 0.65 (65%). Such a deformation behavior is very similar to that obtained in the NC pure Mg specimen (d = 60 nm) prepared by powder metallurgy and deformed in compression at a quasi-static strain rate [19]. However, there is one order of magnitude difference in the grain size between the current specimen and that reported in Ref. [19]. The dramatic decrease of YS and significant increase of tensile elongation in the UFG specimen are believed to be originated from an important change of the dominant deformation mode.

The values of yield strength and total elongation obtained from the engineering stress-strain curves shown in Fig. 4 were plotted against inverse square root of the mean grain size in Fig. 5(a) and (b), respectively. It is very interesting that both plots could be di-

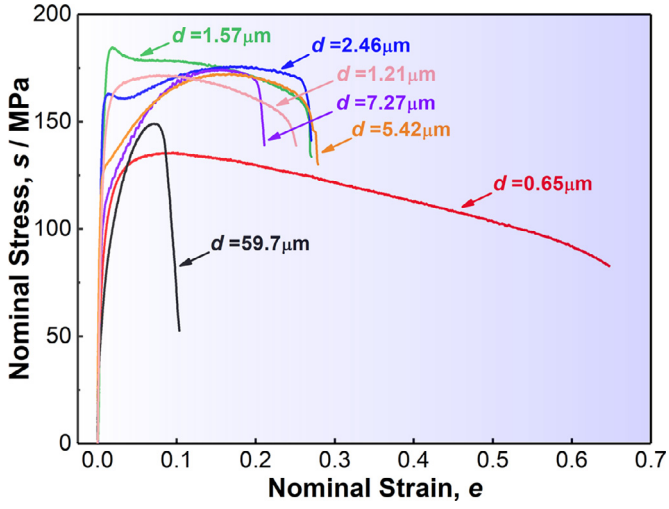

Fig. 4. Nominal stress-strain curves obtained by the room temperature tensile test of the pure Mg specimens having various mean grain sizes (d).

vided into three characteristic regions by the same critical grain sizes. For the specimens with $d \geqq 4.32$ μm (Region I), the yield strength and grain size clearly held a typical Hall-Petch relationship [30, 31] ($\sigma_y = \sigma_0 + kd^{-1/2}$, where σ_y, σ_0 and k are the yield strength, friction stress and Hall-Petch slope, respectively) with a k value of 260 MPa·μm$^{1/2}$ (Fig. 5(a)). The k value obtained in Region I was equivalent to previous results reported in conventionally coarse-grained pure Mg and Mg alloys having strong basal texture [32, 33]. Meanwhile, the total elongation increased almost linearly with decreasing the grain size in Region I, as shown in Fig. 5(b). For the specimens with 1.57 μm $\leqq d <$ 4.32 μm (Region II), the yield strength also increased with decreasing the grain size, but the data points clearly showed negative deviations from the extrapolated Hall-Petch line (the broken line in Fig. 5(a)). Then, the total elongation kept an almost constant value in Region II (Fig. 5(b)). Note that the fine-grained specimens in Region II exhibited good combination of strength and ductility, as was shown in Fig. 4. An inverse Hall-Petch relationship of the yield strength accompanied with a dramatic increase in the tensile elongation was observed when $d <$ 1.57 μm (Region III). A special attention should be paid to the critical grain sizes for realizing the negative deviation of the Hall-Petch slope ($d \sim 4$ μm) and the inverse Hall-Petch effect ($d \sim 1$ μm) acquired in the present bulk pure Mg specimens without impurity contamination, which were considerably coarser than those observed in other metallic materials (usually around several tens of nanometers) [34–36].

3.3. Transition of dominant deformation mode with grain refinement

In order to understand underlying mechanisms that realized the dramatic change of tensile properties (*i.e.*, strength and ductility) with refining the grain size in the present pure Mg, three representative specimens (*i.e.*, the coarse-grained specimen ($d = 7.27$ μm), the fine-grained specimen ($d = 2.46$ μm) and the UFG specimen ($d = 0.65$ μm)) were selected from Region I, II and III, respectively, for characterizing deformation microstructures after tensile deformation to specified strains.

We first focused on deformation twinning. Fig. 6 shows the evolution of the twinning area fraction (f_{twin}) at various tensile strains in the selected specimens. The twinning area fractions were measured by the use of EBSD maps in the way we carried out before [37]. The data points plotted in Fig. 6 represent the average value of three observed areas on each tensile specimen, and differences are shown by the error bars. The insets in Fig. 6 are typical EBSD-IPF maps of the coarse-grained specimen (upper row) and the fine-grained specimen (lower row) at different tensile strains, where only deformation twins were extracted and highlighted. For the coarse-grained specimen, f_{twin} increased sharply with increasing the tensile strain. f_{twin} reached 22.2% at a tensile strain of 0.2. Crystallographic analysis indicated that the twins were exclusively {10–12} extension twins, which rotated the matrix orientation by 86.3° around ⟨1–120⟩ direction and could effectively accommodate the extension stress along ***c***-axis of the matrix [7]. Deformation twinning was dramatically suppressed by the grain refinement. f_{twin} of the fine-grained specimen increased slowly with increasing the tensile strain, but even at a tensile strain of 0.20, f_{twin} was

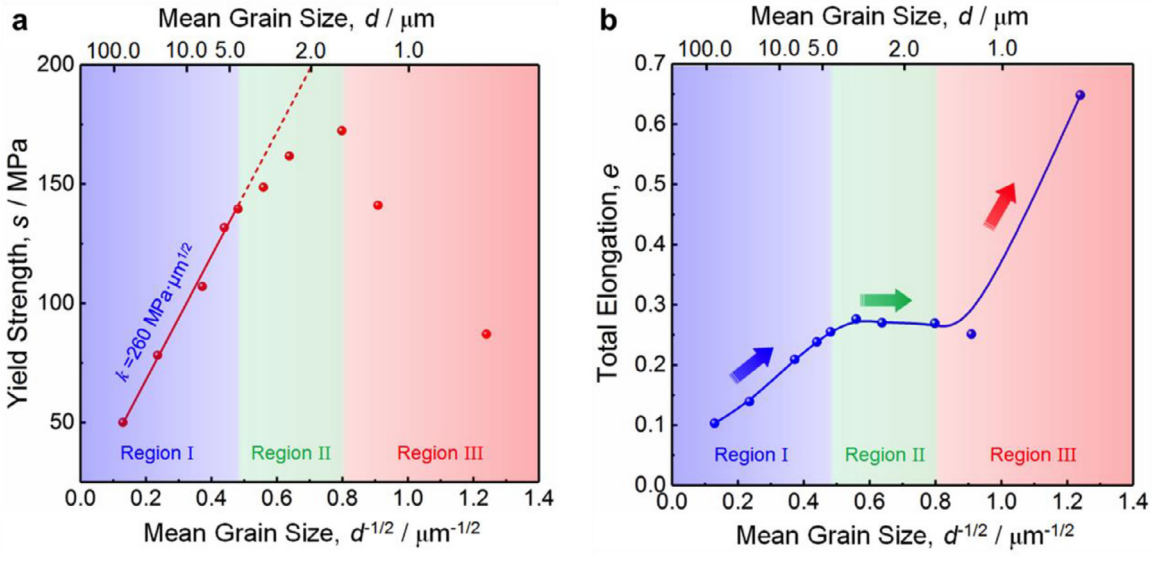

Fig. 5. Grain size dependence of the yield strength and total elongation in the pure Mg having different mean grain sizes. (**a**) Yield strength plotted as a function of inverse square root of the mean grain size. The yield strength followed a typical Hall-Petch relationship in the coarse-grained region (Region I), then the Hall-Petch slope negatively deviated in the fine-grained region (Region II), and eventually exhibited inverse Hall-Petch relationship by further grain refinement (Region III). (**c**) Total elongation plotted as a function of inverse square root of the mean grain size. The total elongation increased almost linearly with decreasing the grain size in Region I, then kept almost constant in Region II, and dramatically increased in Region III.

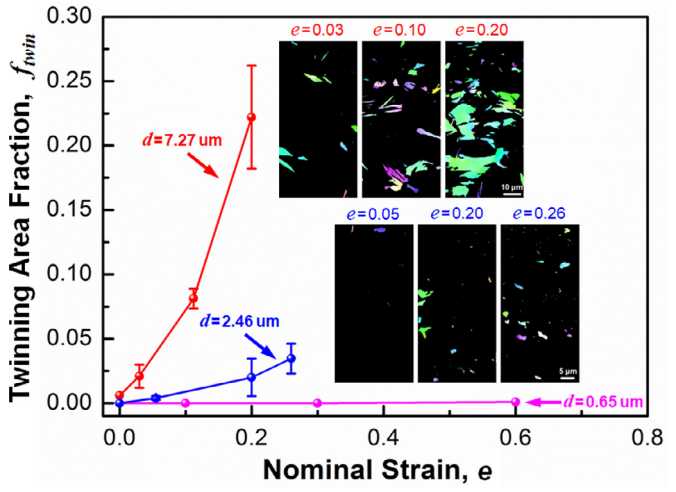

Fig. 6. Twinning area fractions at different tensile strains in the specimens having different mean grain sizes corresponding to Region I, II and III shown in Fig. 5. The graph exhibits the grain size dependence of deformation twinning. The twinning area fractions were measured from EBSD maps in the way we carried out for a Mg alloy in previous study [37]. The deformation twinning was significantly suppressed with decreasing the grain size. The insets are typical EBSD-IPF maps extracting only twinning areas in the coarse-grained (d = 7.27 μm, upper row) and the fine-grained (d = 2.46 μm, lower row) specimens at various tensile strains. The UFG specimen (d = 0.65 μm) did not show deformation twins at all.

only 2.0%, which was much smaller than that of the coarse-grained specimen at the same tensile strain level (f_{twin} = 22.2%). In the UFG specimen, deformation twinning was completely suppressed. Deformation twins could not be observed even after careful EBSD observations (EBSD-IPF maps are not shown here) during the entire tensile deformation process.

Although deformation twinning was dramatically suppressed in the fine-grained and UFG specimens, they exhibited better ductility than that of the coarse-grained specimens located in Region I (Fig. 5(b)). If only basal $\langle \boldsymbol{a} \rangle$ slips occurred in the fine-grained and UFG specimens, the deformation in each grain would be 2-dimensional and the better ductility could not be realized. There must be some other deformation mechanisms responsible for the enhanced ductility in those specimens. In our previous study, we observed simultaneously enhanced strength and ductility in a commercial Mg alloy (ZKX600) by the grain refinement from 23.3 μm to 0.77 μm [29, 37]. We found that the enhanced ductility was attributed to the activation of non-basal slip systems having $\langle \boldsymbol{c} \rangle$ component Burgers vectors, which played an important role in accommodating plastic strains along $\langle \boldsymbol{c} \rangle$ axis in each grain [37]. On the other hand, it is also known that the occurrence of grain boundary mediated deformation mechanisms (such as grain rotation or/and GBS) could improve the ductility of various kinds of materials. Koike et al. [9] reported that GBS occurred in a fine-grained AZ31 Mg alloy even at room temperature. The plastic strain accommodated by GBS was measured to be 8% of the total plastic strain in the AZ31 Mg having a mean grain size of 8 μm which was tensile tested at a quasi-static strain rate of 8.3 $\times$ 10^{-4} s^{-1} at room temperature (300 K). Thus, the present fine-grained and UFG specimens were subjected to further microstructural observations, for revealing their underlying deformation mechanisms.

Figure 7 **(a)** shows a SEM micrograph of the fine-grained specimen tensile deformed to a strain of 0.05. The surface of the specimen was electro-polished before the tensile test. A white line horizontally crossing the center of the image was introduced by FIB prior to the tensile test. Tensile direction was parallel to the horizontal direction of the image. Straight and parallel slip lines indicated by yellow arrows were observed within many grains after a tensile strain of 0.05, indicating dislocation slips played an important role for the plastic deformation. On the other hand, as indicated by red arrows in Fig. 7(a), offsets of the scribed line at grain boundaries were also observed, which was associated with the occurrence of GBS [9, 38]. Note that the offsets could only be found in a small number of grain boundaries, suggesting that the occurrence of GBS was still not dominant and depended on grain boundary characters. The identical area shown in Fig.7 (a) was observed again after deformation to a strain of 0.20 without polishing. The grains were clearly elongated along the tensile direction, indicating plastic deformation governed by dislocation slips and twinning. The scribed FIB line looked discontinuous even within grains due to surface steps introduced by dislocation slips.

The fine-grained specimen was also observed by TEM to distinguish the types of operated dislocations (<$\boldsymbol{a}$> type with $\boldsymbol{b}$ = 1/3<11−20>, pyramidal $\langle \boldsymbol{c}+\boldsymbol{a} \rangle$ type with $\boldsymbol{b}$ = 1/3<11−23>, where $\boldsymbol{b}$ is Burgers vector). Fig. 7(c) represents a typical grain after a tensile strain of 0.05, observed from near [11-20] zone axis by minimum tilting in TEM. As indicated by the SAD pattern inserted in Fig. 7(c), the basal plane of this grain was aligned parallel to the incident beam direction, so that the basal plane was edge on. Profuse dislocations were produced by tensile deformation and they were aligned roughly parallel to the trace of the basal plane indicated by a red dashed line. These dislocations lying parallel to the basal traces were most likely basal $\langle \boldsymbol{a} \rangle$ dislocations. Besides, some curved dislocation segments (indicated by yellow arrows) extending out of the basal traces could be also observed by careful inspection, implying some non-basal slip systems were also activated. To analyze the nature of the Burgers vector of these dislocations, this grain was further observed from near [11-20] zone axis under two beam conditions with $\boldsymbol{g}$ = 0002, as shown in Fig. 7(d). According to the "$\boldsymbol{g}\cdot\boldsymbol{b}$ = 0″ invisibility criterion [39], dislocations having $\langle \boldsymbol{a} \rangle$ component should be out of contrast and only $\langle \boldsymbol{c} \rangle$ component could be observed. Fig. 7(d) is totally free of any dislocation contrast. That means, besides basal dislocations, non-basal $\langle \boldsymbol{a} \rangle$ dislocations were activated in the fine-grained specimen at the beginning of plastic deformation. We have checked many grains and all of them showed similar dislocation configurations and characters. Therefore, it can be concluded that dislocation slips dominated plastic deformation of the fine-grained specimen. GBS and deformation twinning, as supplementary deformation mechanisms, also contributed to the plastic flow in part. As a result, the tensile ductility of the fine-grained specimen was larger than that of the coarse-grained counterpart, but the yield strength was negatively deviated from the Hall-Petch relationship in Region I.

Fig. 8 shows deformation microstructures of the UFG specimen. Fig. 8(a) is a SEM image of a polished surface in the UFG specimen after deformation to a tensile strain of 0.10. Different from the results of the fine-grained specimen (Fig. 7(a) and (b)), slip lines could not be observed within grains and the scribed line remained straight within each individual grain. On the other hand, abrupt offsets of the scribed line at grain boundaries indicated by the red arrows were frequently observed in Fig. 8(b), which was an enlarged image of the boxed region in **(a)**. After further deformation to a tensile strain of 0.30 (Fig. 8(c) and (d)), slip lines still could not be recognized. Since the identical area was observed, the major difference between Fig. 8(b) and (d) was the clearly expanded displacement of the scribed line at grain boundaries. The results indicated that GBS occurred more dominantly in the UFG specimen. Bell and Langdon [40] have proposed an equation for estimating the strain accommodated by GBS (e_{GBS}),

$$e_{\text{GBS}} = \frac{\mu}{d} \tag{1}$$

where μ is a component of GBS displacement parallel to the tensile direction. We have measured about 50 grain boundaries that

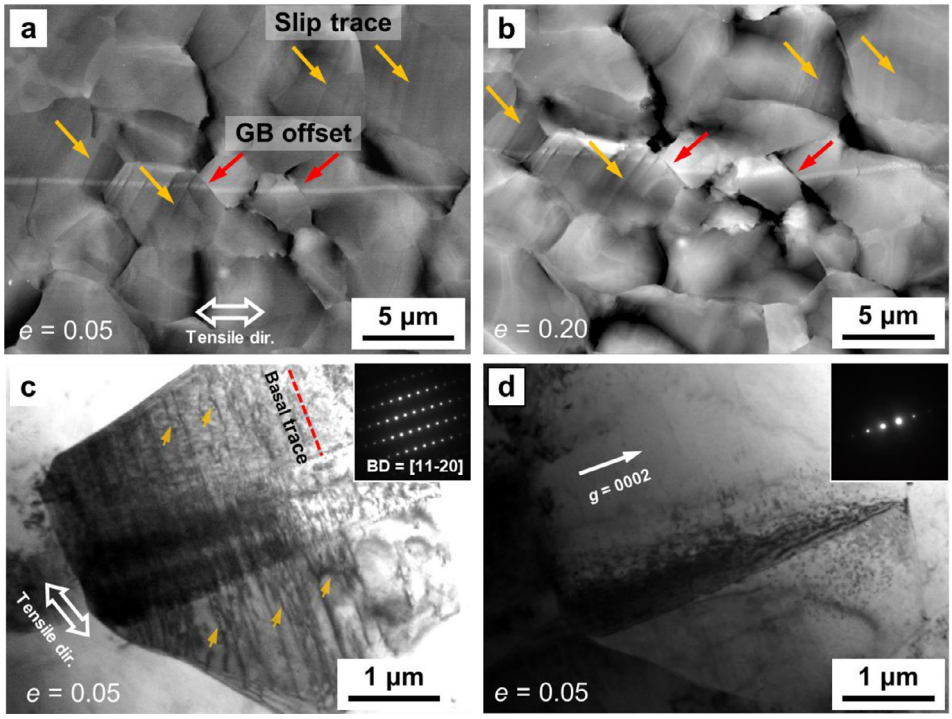

Fig. 7. Deformation microstructures after tensile deformation of the fine-grained specimen ($d = 2.46\ \mu$m). (**a**) and **(b)** are SEM images at strains of 0.05 and 0.20, respectively, showing profuse slip traces (indicated by yellow arrows) and offsets of the scribed FIB line at grain boundaries (indicated by red arrows). (**c**) BF-TEM image of a typical grain at a strain of 0.05 observed along [11-20] zone axis, showing profuse dislocations aligned parallel to basal traces indicated by the red broken line. Some dislocation segments deviated from the basal traces are indicated by yellow arrows. **(d)** BF-TEM image of the same grain acquired under two beam condition with $\boldsymbol{g} = 0002$, showing no dislocation contrast.

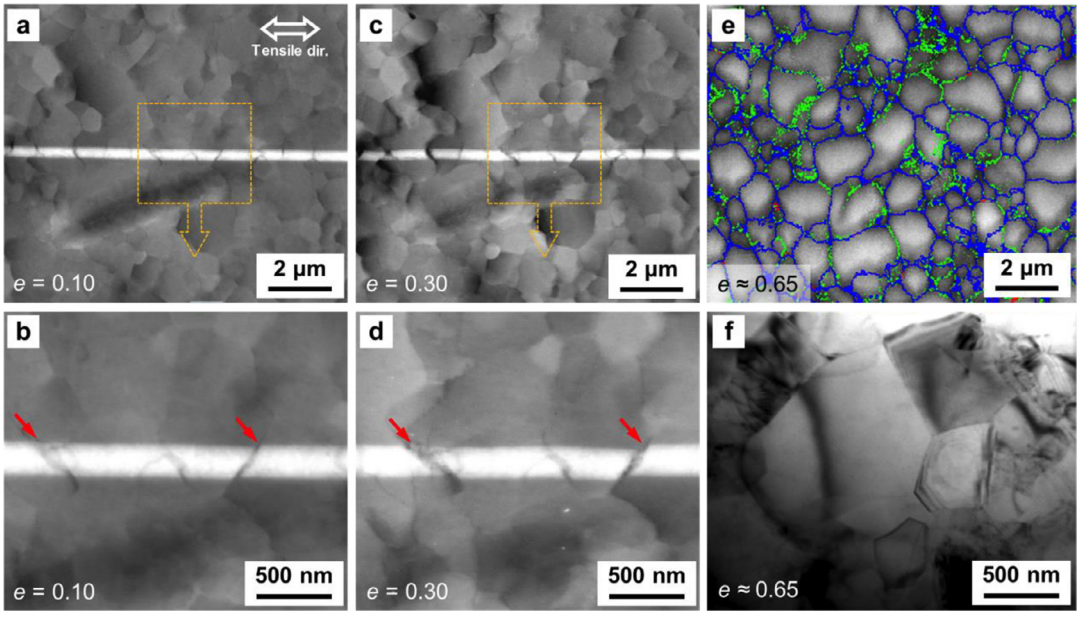

Fig. 8. Deformation microstructures after tensile deformation of the UFG specimen ($d = 0.65\ \mu$m). (**a-d**) are SEM images of the identical specimen surface at strains of 0.10 (**a, b**) and 0.30 (**c, d**), respectively, showing obvious offsets of the scribed line at grain boundaries (indicated by red arrows). (**e, f**) EBSD-GB map and BF-TEM image of the UFG specimen after tensile fracture, obtained in the vicinity of the fracture surface, showing equiaxed grains and low density of dislocations, respectively. The tensile direction was parallel to the horizontal direction for all the images.

showed shifts of scribed lines after deformation to a strain of 0.3, and the average μ value was about 0.14 μm. Therefore, the e_{GBS} was as high as 0.21, which took 70% of the total plastic strain (0.3). Fig. 8(e) and (f) show an EBSD-GB map and a BF-TEM image, respectively, of the UFG specimen after tensile deformation to failure. The observed areas were in the vicinity of the fracture surface and the tensile direction was along the horizontal direction for both images. Interestingly, equiaxed grains could be still observed after experiencing such a large tensile strain of 0.65 (Fig. 8(e)) but the dislocation density within equiaxed grains seemed very low (Fig. 8(f)).

We also performed strain rate jump test on several typical specimens, where the imposed strain rate was changed repeatedly from $\dot{\varepsilon}_1$=8.3 × 10^{-4} s^{-1} to $\dot{\varepsilon}_2$=8.3 × 10^{-3} s^{-1}. As shown in Fig. 9(a), the

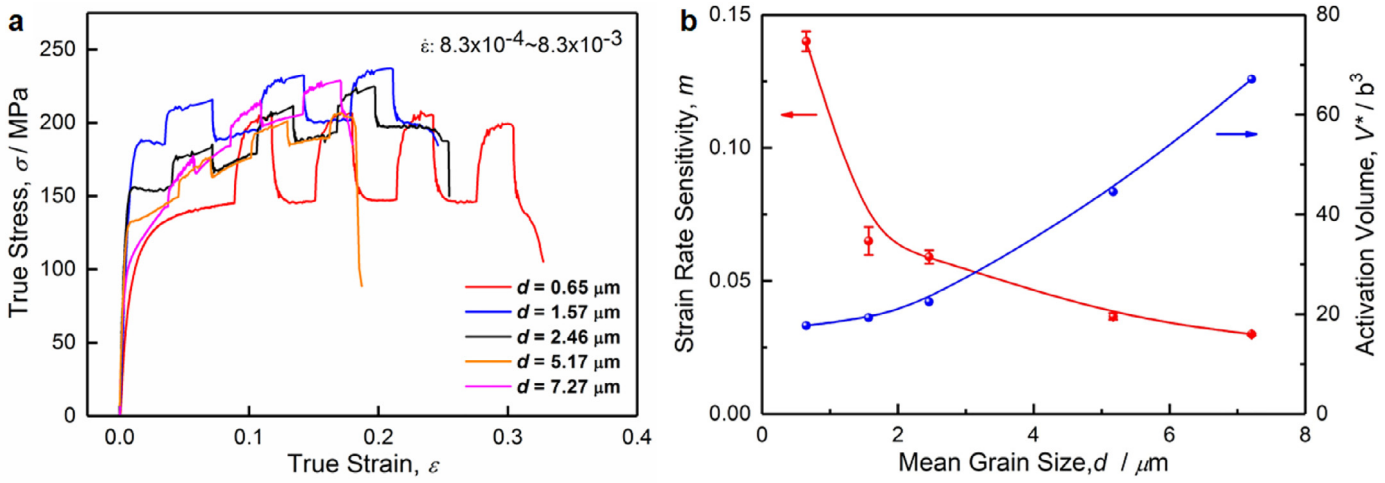

Fig. 9. Results of the strain rate jump test for representative specimens with different grain sizes. (**a**) Ture stress-true strain curves obtained by the strain rate jump test. The steps on the σ-ε curves show changes in the flow stress σ caused by the strain rate jump between 8.3 × 10^{-4} s^{-1} and 8.3 × 10^{-3} s^{-1}. (**b**) The evolution of strain rate sensitivity (m) and activation volume (V^*) as a function of mean grain size.

specimens with different grain sizes exhibited different responses in the flow stress to the changes of the strain rate. It is well-known that the strain rate sensitivity (m) of the flow stress can be calculated by the equation shown below,

$$m = \frac{\partial \ln \sigma}{\partial \ln \dot{\varepsilon}} = \frac{1}{\sigma}\frac{\partial \sigma}{\partial \ln \dot{\varepsilon}} \tag{2}$$

where $\dot{\varepsilon}$and $\sigma$are the strain rate and flow stress, respectively. For the jump test, the equation can be written as,

$$m = \frac{(\sigma_2 - \sigma_1)}{[(\sigma_2 + \sigma_1)/2]\ln(\dot{\varepsilon}_2/\dot{\varepsilon}_1)} \tag{3}$$

where $\sigma_1$and $\sigma_2$are the flow stresses under the strain rates of $\dot{\varepsilon}_1$ and $\dot{\varepsilon}_2$, respectively [41, 42]. The calculated m values were plotted against the average grain size in Fig. 9(b). For the coarse-grained specimen with the mean grain size of 7.27 μm, the m value was about 0.03, which was the same as that of an as-cast pure Mg with a very coarse grain size (several hundreds of micrometers) reported by Figueiredo et al. [43]. The m value increased monotonously with the grain refinement. Note that there seems to be the critical grain size around 1 μm, below which the m value raised significantly. The m value of the UFG specimen (d = 0.65 μm) reached about 0.14, which was much higher than that of the fine-grained specimens (*e.g.*, m = 0.06 for the specimen with d = 2.46 μm), but approached to a magnitude for the materials showing superplasticity [44].

The activation volume (V^*) can be calculated using the equation shown below [17, 19, 45],

$$V^* = \frac{MkT}{\sigma m} \tag{4}$$

where M is the Taylor factor (we set $M = \sqrt{3}$ for simplicity), k is the Boltzmann constant (k = 1.38 × 10^{-23} J/K), T is the absolute temperature in Kelvin (T = 298 K) and σ is the tensile yield stress. As plotted in Fig. 9(b), the activation volume decreased gradually with the grain refinement, and a very small V^* value of 17.7 b^3 was obtained in the UFG specimen, where b is the magnitude of the Burgers vector for basal slip in Mg (b = 3.21 × 10^{-10} m). It has been reported that the V^* value for conventional coarse-grained pure Mg (d = 120 μm) deformed at room temperature was about 409 b^3, because forest dislocation dominated the plastic deformation, leading to a negligible strain rate sensitivity and a high activation volume [19, 45]. On the other hand, the activation volume decreases substantially when GBS becomes dominating. For instance, it has been reported in ultrafine grained Mg deformed at high temperatures that the activation volume can be as low as ~1 b^3 [19]. Therefore, it is again considered that GBS played a major role in giving the plastic flow in the present UFG pure Mg specimen and was responsible to the large tensile elongation in Region III.

4. Discussion

4.1. Grain size dependence of critical shear stress for various deformation modes

To clarify the origin for the switch of dominant deformation modes by changing the grain size, we here consider the grain size dependence of the critical shear stress for activating three kinds of competing mechanisms of plastic deformation, *i.e.*, deformation twinning, dislocation slips and GBS. It is considered that the plastic deformation mechanism having the lowest critical shear stress would become the dominant one at a specific grain size. Additionally, the ability of arbitrary deformation is also considered as an essential condition for plastic deformation, because the activation of dislocation slips is anisotropic in HCP Mg crystal. Although basal $\langle \boldsymbol{a} \rangle$ slip is usually dominant in Mg, it can realize only 2-dimensional deformation in each grain. Thus, we emphasize other deformation modes in addition to the basal slip in the consideration, for satisfying the von Mises criterion [46].

First, we demonstrate the critical shear stress for the dislocation-mediated plasticity. It is well known that the Hall-Petch relationship stands for the yield strength of most metallic materials when the dislocation slip is the mechanism for plastic deformation [47]. Thus, the grain size dependence of the critical shear stress for activating the dislocation-mediated plasticity (τ_D) could be expressed as,

$$\tau_D = \tau_{0,D} + k_D d^{-1/2} \tag{5}$$

where $\tau_{0,D}$ is the shear stress when the grain size is very large, and k_D is the Hall-Petch constant (slope). According to the experimental results obtained in previous studies using single crystal, the critical shear stress for basal, prismatic and pyramidal slips are ~1 MPa, ~39 MPa and ~80 MPa, respectively [48]. Although the Hall-Petch relationship is an empirical relationship, several kinds of models have been proposed for theoretically explaining it [49, 50]. Among them, the dislocation pile-up model is the most cogent one. The dislocation pile-up model considers that macroscopic

yielding of polycrystalline metals starts when the stress concentration by pile-up of dislocations at a grain boundary reaches the critical value (τ_c) to activate dislocation slips in the neighboring grain. It has been reported that in recrystallized UFG metals or nanocrystalline materials the dislocation emission from grain boundary is critical to start macroscopic plastic deformation [29, 51, 52]. Based on the stress concentration due to pile-up of dislocations at grain boundary, k_D could be expressed as [47],

$$k_D = \sqrt{\frac{\tau_c^{GB} C \mu b}{\beta}} \tag{6}$$

where τ_c^{GB} is the critical shear stress for the dislocation emission from grain boundary, μ is the shear modulus, b is the magnitude of the Burgers vector of dislocation of a certain slip system, and C and β are material constants. τ_c^{GB} can be approximately set equal to the ideal shear strength of the crystal [53]. The shear moduls, μ, can be calculated from the experimental elastic constants [54]. For the ring dislocation pile-up model [55],

$$C = \frac{\pi(2-\nu)}{4(1-\nu)} \tag{7}$$

where $\nu = 0.33$ is the Poisson ratio and $\beta = 0.5$.

Next, we consider the critical shear stress for activating the twinning-mediated plasticity. The critical event in twinning is the nucleation of twin, because the local stress required to nucleate twin is much higher than that for growth of the twin [56]. The GB acts as one of the candidates of nucleation site for twinning, as have been observed by many researchers (like [29]). But the nucleation mechanism of twin has not been fully understood due to complicated collective slips or collective motion of atoms including shuffling necessary for twinning in HCP Mg [57]. However, it has been known that the yielding controlled by twinning also follows the Hall-Petch type relationship, but with a larger slope (k_T) than that controlled by dislocation slips [11]. Thus, we use the Hall-Petch type equation also for evaluating the grain size dependence of the critical shear stress for twinning, and adopt the present experimental values of k_T obtained in Region I (Fig. 5) and $\tau_0^T \approx 5$ MPa taken from Ref. [58] to characterize the critical shear stress to activate the twinning-mediated plasticity.

Finally, for the GB-mediated plasticity, the GBS can be considered as a GB shear [59]. For the grain size dependence of the critical shear stress in this case, the relationship used by Argon and Yip [59, 60] shown below can be adopted,

$$\tau_c(\mathrm{GB}) = \tau_{is}^{GB}\left[1 + \ln\left(\frac{\dot{\gamma}_{GB} d}{6\delta\gamma^T \upsilon_D}\right) \times \frac{kT}{Q_\nu}\right] \tag{8}$$

where τ_{is}^{GB} is the ideal GB shear resistance for HAGBs in Mg and is approximately set to half of the ideal shear strength (τ_{is}) of pure Mg. τ_{is}= 1.84 GPa has been given from first-principles calculations [53], $\dot{\gamma}_{GB}$= 8.3 × 10^{-4} s^{-1} is the strain rate due to GB shear, δ is the typical width of GBs which is approximately equal to the magnitude of Burgers vector (3.21 Å), $\gamma^T \approx 0.025$ is the typical shear strain at yielding, υ_D= 10^{14} s^{-1} is the atomic vibration frequency, k is the Boltzmann constant, T is the absolute temperature and Q_ν= 1.0 eV is the activation energy for GB diffusion [61].

The grain size dependence of the critical shear stresses for three kinds of deformation mechanisms at room temperature is shown in Fig. 10. Generally, it is considered that, at a given grain size, the deformation mechanisms with the lowest critical shear stress should dominate the plastic deformation. As shown in Fig. 10, basal slip system exhibits the lowest critical shear stress when the grain size is in the range of several tens of micrometers. As has been mentioned above, however, basal slips can realize only 2-dimensional deformation in each grain. According to the von Mises criterion [46], five independent slip (or twinning) systems is required for arbitrary deformation of polycrystalline materials. {10–12} extension twinning is expected to be easily activated since it possesses the second lowest critical shear stress in the region of coarse grain sizes. Thus, twinning is also the dominant and important plastic deformation mechanism in the range of coarse grain sizes. With decreasing the grain size, the critical shear stresses required to activate various dislocation slip systems and {10–12} twinning increase. However, the critical shear stress for {10–12} twinning exhibits a stronger grain size dependence than those for dislocation slips, and the critical shear stress for prismatic ⟨**a**⟩ slip becomes lower than that of {10–12} twinning at a critical grain size of d_{c1} = 3.2 μm. This is in good agreement with the current experimental result of the deformation microstructure observed in the fine-grained specimen with a mean grain size of 2.46 μm, where a significant suppression of deformation twinning and the activation of non-basal (probably prismatic) ⟨**a**⟩ dislocations were confirmed (Fig. 7). On the other hand, the critical shear stress for GB shear (GBS) deceases sharply with decreasing the grain size. Further decrease of the grain size shows another critical grain size of d_{c2} = 0.9 μm in Fig. 10, below which the critical shear stress for GB shear becomes lower than that for the basal slip. This also agrees well with the present experimental result that dislocation slips were greatly suppressed while GBS became dominant in the UFG specimen having a mean grain size of 0.65 μm. Then, the three kinds of mechanisms contribute together to the plastic deformation of pure Mg when the average grain size is between d_{c1} and d_{c2}. This is considered as a transition region. For the UFG specimens with the mean grain size below d_{c2}, the GB-mediated plasticity (*i.e.*, GBS) becomes the predominant deformation mechanism according to Fig. 10, which is consistent with our experimental results, where the inverse Hall-Petch relationship and the exceptional large tensile elongation were observed (Fig. 4). Note that the texture effect was not taken into account in the present model, although mechanical properties of Mg are significantly affected by textures. This is because the critical "shear" stresses which are not affected by crystal orientation (texture) are considered for each dislocation slip and twinning (Fig. 10). The critical

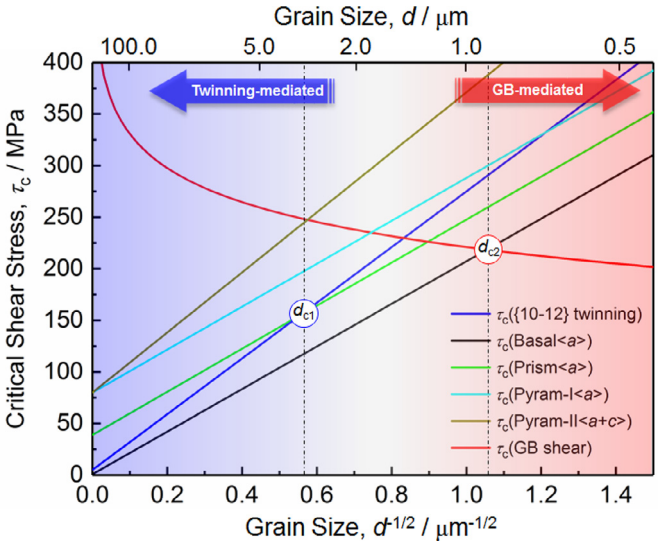

Fig. 10. Grain size dependence of the critical shear stresses for {10–12} deformation twinning, various dislocation slip systems and GB shear in pure Mg. These deformation mechanisms exhibit different grain size dependencies, which results in two critical grain sizes, d_{C1} = 3.2 μm and d_{C2} = 0.9 μm. When $d > d_{C1}$, the plastic deformation is mainly mediated by deformation twinning; when $d < d_{C2}$, the plastic deformation is mainly mediated by GB shear (GB sliding); when $d_{C1} > d > d_{C2}$, a transition region appears, where several deformation mechanisms operate simultaneously.

stress for GB shear is unlikely to be affected by texture. Zeng et al. [17] have reported that the inter-granular deformation mechanisms became dominant in pure Mg under compression at room temperature when the average grain size was reduced to the vicinity of 1 μm, even though their specimen was prepared by low-speed warm extrusion and exhibited totally different texture from the present specimens. Consequently, we can conclude that the current theoretical consideration for the critical shear stress (summarized in Fig. 10) explained the transition of the dominant deformation modes in the pure Mg specimens having different average grain sizes as well as the change of their experimentally obtained mechanical properties in three distinct grain size regions (Regions I, II and III) shown in Fig. 5 very well. The present understanding would be also applicable to UFG Mg processed by other methods.

4.2. Tailoring the grain boundary stability of bulk ufg mg

It is an important and new finding that 1 μm is the critical grain size in bulk pure Mg free from impurity contamination, below which the GB-mediated deformation mechanism (*i.e.*, GBS) is significantly enhanced, leading to the obvious softening of the strength and the dramatic improvement of ductility. As a result, critical shortcomings of Mg, such as lack of sufficient number of independent slip systems and strong basal texture that lead to the poor room temperature ductility and formability, become less important or even negligible.

The critical grain size ($d \sim 1$ μm) for initiating the GB-mediated plasticity in pure Mg are nearly two orders of magnitude larger than those in other metals [34–36]. For instance, the critical grain size for realizing softening of strength in Ni is as small as 10 nm [34]. Although the reason for such a large critical grain size in Mg is not clearly understood, we think it is probably caused by the following reasons: (i) GBS is a thermally activated process. The melting temperature of Mg (923 K) is much lower than those of other metals widely studied (such as Cu, Fe and Ni). As a result, room temperature deformation of Mg corresponds to a higher homologous temperature (T/T_m, where T_m is the melting temperature) than other metals. (ii) GBS is a kind of the creep process controlled by grain boundary diffusion. The activation energy for grain boundary diffusion (Q) in Mg is ~92 kJ mol^{-1}, which is much lower than those of other metals widely studied [62]. In addition, it has been reported that Q can furthermore decrease to ~75 kJ mol^{-1} in UFG Mg [43]. (iii) Eq. (8) indicates that the critical shear stress for GBS is proportional to the value of τ_{is}^{GB}, which is approximately equal to the half of the ideal shear strength (τ_{is}). First-principle calculation suggested that τ_{is} is 1.84 GPa for Mg, 2.16 GPa for Cu and 3.17 GPa for Ni [53]. Thus, the critical grain size for changing the deformation mechanism into GBS in Mg should be larger than those of other metals such as Cu and Ni.

Besides the grain size, we would like to suggest that the grain boundary property for the GB-mediated plasticity could be tailored through an addition of alloying elements. Recently, we found that bulk UFG ($d = 0.25$ μm) Mg-0.3at.%Zn dilute alloy processed by HPT exhibited very high strength (tensile strength ~250 MPa) but quite limited ductility (premature fracture before yielding, unpublished work [63]), which were dramatically different from the results in the UFG pure Mg shown in this paper. Microstructure observation suggested that Zn atoms were segregated at grain boundaries newly formed during HPT. Similar phenomenon has also been observed by Basha et al. [64] in an UFG Mg-Zn-Y alloy processed by HPT. It is generally believed that the segregation of alloying elements could decrease the grain boundary energy and, thus, stabilize the grain boundary [65]. In contrast, Somekawa et al. [66–68] have shown that the grain boundary mobility of Mg could be enhanced by trace addition of some alloying elements. For example, Somekawa et al. [66] found that the elongation-to-failure of a fine-grained Mg-0.3at.%Mn alloy ($d = 3.0$ μm) prepared by hot extrusion was as high as 0.64 (64%), which was more than twice as that of pure Mg having a similar grain size tensile tested under the same condition. Segregation of Mn atoms to grain boundaries was also observed in Mg-Mn binary alloy. However, the underlying mechanisms for the enhanced grain boundary mobility due to GB segregation of Mn are still unclear and the mechanical properties of bulk UFG Mg-Mn binary alloy have not been explored yet. Nevertheless, these results suggest that the grain boundary mobility of bulk UFG Mg can be furthermore optimized by the addition of appropriate alloying elements. We believe that, if combined with a proper alloy design strategy, the findings in the present paper have a great importance for the development of strong and ductile Mg alloys for future practical applications.

5. Conclusions

In summary, we have revealed in this paper that the grain size plays a crucial role in changing the dominant deformation modes in pure Mg at room temperature and, therefore, the grain size determines the strength and ductility of the material. The main conclusions obtained in the present study are as follows:

(1) Bulk contamination-free polycrystalline pure Mg specimens having fully recrystallized microstructures with a wide range of average grain sizes ranging from 0.65 μm to 59.7 μm were successfully fabricated by HPT and subsequent annealing. It should be noted that the grain size of 0.65 μm is the smallest grain size ever reported in pure Mg in fully recrystallized state.
(2) Deformation twinning mediated the plastic deformation in the conventional coarse-grained specimens, which led to the low yield strength, strong work-hardening and limited ductility of the specimens.
(3) Deformation twinning was significantly suppressed when the grain size was refined down to 3–4 μm, and non-basal dislocation slip systems having $\langle \boldsymbol{a} \rangle$ Burgers vector were activated. GBS also contributed to the plastic deformation in part, which led to the negative deviation from the Hall-Petch relationship and the increase of tensile ductility.
(4) GBS governed the plastic deformation in the UFG specimen with a sub-micrometer grain size, which led to softening (inverse Hall-Petch effect) and exceptionally large room temperature tensile elongation up to 0.65 (65%) at a quasi-static strain rate of 8.3×10^{-4} s^{-1}.
(5) The transition of dominant deformation modes with the grain refinement in bulk polycrystalline pure Mg could be consistently explained by the model showing the distinct grain size dependence of the critical shear stress for different deformation modes, *i.e.*, dislocation slips, deformation twinning, and GBS.
(6) The critical grain sizes for realizing the transition of dominant deformation modes in pure Mg were considerably coarser than those reported in other metals, which would make it possible to design strong and ductile Mg alloys for future practical applications.

Declaration of Competing Interest

The authors declare that they have no known competing financial interests or personal relationships that could have appeared to influence the work reported in this paper.

Acknowledgments

This work was financially supported by the Elements Strategy Initiative for Structural Materials (ESISM, No. JPMXP0112101000), the Grant-in-Aid for Scientific Research (S) (No. 15H05767), and the

Grant-in-Aid for Challenging Exploratory Research (No. 18K18945), all through the Ministry of Education, Culture, Sports, Science and Technology (MEXT), Japan. NT was also supported by JST CREST (JPMJCR1994) and Light Metal Edudational Foundation. SO was also supported by Grant-in-Aid for Scientific Research (A) (Nos. 17H01238 and 23246025). HS was supported by the Grain-in-Aid for Scientific Research (C) (No. 19K05068). RXZ appreciates the support from National Natural Science Foundation of China (No. 51901007) and Youth Talent Support Program of Beihang University. The authors gratefully thank Prof. Atul H. Chokshi of Indian Institute of Science for his good advices and discussions during his stay in Kyoto University.

Supplementary materials

Supplementary material associated with this article can be found, in the online version, at doi:10.1016/j.actamat.2020.07.055.

References

[1] B.C. Suh, M.S. Shim, K.S. Shin, N.J. Kim, Current issues in magnesium sheet alloys: where do we go from here, Scr. Mater. 84-85 (2014) 1–6.
[2] M. Easton, A. Beer, M. Barnett, C. Davies, G. Dunlop, Y. Durandet, S. Blacket, T. Hilditch, P. Beggs, Magnesium alloy applications in automotive structures, JOM 60 (2008) 57–62.
[3] W. Xu, N. Birbilis, G. Sha, Y. Wang, J.E. Daniels, Y. Xiao, A high-specific-strength and corrosion-resistant magnesium alloy, Nature Mater 14 (2015) 1229–1235.
[4] J. Koike, T. Kobayashi, T. Mukai, H. Watanabe, M. Suzuki, K. Maruyama, K. Higashi, The activity of non-basal slip systems and dynamic recovery at room temperature in fine-grained AZ31B magnesium alloys, Acta Mater 51 (2003) 2055.
[5] Z. Wu, W.A. Curtin, The origins of high hardening and low ductility in magnesium, Nature 526 (2015) 62–67.
[6] W.B. Hutchinson, M.R. Barnett, Effective values of critical resolved shear stress for slip in polycrystalline magnesium and other hcp metals, Scr. Mater. 63 (2010) 737–740.
[7] M.R. Barnett, Twinning and the ductility of magnesium alloys: part I: “Tension” twins, Mater. Sci. Eng. A 464 (2007) 1–7.
[8] M.R. Barnett, Twinning and the ductility of magnesium alloys: part II: “Contraction” twins, Mater. Sci. Eng. A 464 (2007) 8–16.
[9] J. Koike, R. Ohyama, T. Kobayashi, M. Suzuki, K. Maruyama, Grain-boundary sliding in AZ31 magnesium alloys at room temperature to 523 K, Mater. Trans. 44 (2003) 445–451.
[10] D. Ando, Y. Sutou, J. Koike, Internal microstructure observation of enhanced grain-boundary sliding at room temperature in AZ31 magnesium alloy, Mater. Sci. Eng. A 666 (2016) 94–99.
[11] M.A. Meyers, O. Vöhringer, V.A. Lubarda, The onset of twinning in metals: a constitutive description, Acta Mater 49 (2001) 4025–4039.
[12] Q. Yu, Z.W. Shan, J. Li, X. Huang, L. Xiao, J. Sun, E. Ma, Strong crystal size effect on deformation twinning, Nature 463 (2010) 335–338.
[13] Q. Yu, L. Qi, R.K. Mishra, J. Li, A.M. Minor, Reducing deformation anisotropy to achieve ultrahigh strength and ductility in Mg at the nanoscale, Proc. Natl. Acad. Sci. 110 (2013) 13289–13293.
[14] S. Biswas, S. Suwas, Evolution of sub-micron grain size and weak texture in magnesium alloy Mg-3Al-0.4Mn by a modified multi-axial forging process, Scr. Mater 66 (2012) 89–92.
[15] M.R. Barnett, Z. Keshavarz, A.G. Beer, D. Atwell, Influence of grain size on the compressive deformation of wrought Mg-3Al-1 Zn, Acta Mater 52 (2004) 5093–5103.
[16] Q. Yang, A.K. Ghosh, Deformation behavior of ultrafine-grain (UFG) AZ31B Mg alloy at room temperature, Acta Mater 54 (2006) 5159–5170.
[17] Z. Zeng, J.F. Nie, S.W. Xu, C.H. Davies, N. Birbilis, Super-formable pure magnesium at room temperature, Nature Commun 8 (2017) 972.
[18] H. Somekawa, T. Mukai, Hall-Petch breakdown in fine-grained pure magnesium at low strain rates, Metall. Mater. Trans. A 46 (2015) 894–902.
[19] H.J. Choi, Y. Kim, J.H. Shin, D.H. Bae, Deformation behavior of magnesium in the grain size spectrum from nano-to micrometer, Mater. Sci. Eng. A 527 (2010) 1565–1570.
[20] P.R. Cetlin, M.T.P. Aguilar, R.B. Figueiredo, T.G. Langdon, Avoiding cracks and inhomogeneities in billets processed by ECAP, J. Mater. Sci. 45 (2010) 4561–4570.
[21] R. Zheng, T. Bhattacharjee, A. Shibata, T. Sasaki, K. Hono, M. Joshi, N. Tsuji, Simultaneously enhanced strength and ductility of Mg-Zn-Zr-Ca alloy with fully recrystallized ultrafine grained structures, Scr. Mater. 131 (2017) 1–5.
[22] K. Edalati, A. Yamamoto, Z. Horita, T. Ishihara, High-pressure torsion of pure magnesium: evolution of mechanical properties, microstructures and hydrogen storage capacity with equivalent strain, Scr. Mater. 64 (2011) 880–883.
[23] R.B. Figueiredo, S. Sabbaghianrad, A. Giwa, J.R. Greer, T.G. Langdon, Evidence for exceptional low temperature ductility in polycrystalline magnesium processed by severe plastic deformation, Acta Mater 122 (2017) 322–331.
[24] L. Zhao, N. Park, Y. Tian, S. Chen, A. Shibata, N. Tsuji, Novel thermomechanical processing methods for achieving ultragrain refinement of low-carbon steel without heavy plastic deformation, Mater. Res. Lett. 5 (2017) 61–68.
[25] N. Tsuji, Y. Ito, Y. Saito, Y. Minamino, Strength and ductility of ultrafine grained aluminum and iron produced by ARB and annealing, Scr. Mater. 47 (2002) 893–899.
[26] N. Kamikawa, X. Huang, N. Tsuji, N. Hansen, Strengthening mechanisms in nanostructured high-purity aluminium deformed to high strain and annealed, Acta Mater 57 (2007) 4198–4208.
[27] Y.Z. Tian, S. Gao, L.J. Zhao, S. Lu, R. Pippan, Z.F. Zhang, N. Tsuji, Remarkable transitions of yield behavior and Lüders deformation in pure Cu by changing grain sizes, Scr. Mater. 142 (2018) 88–91.
[28] S. Gao, M. Chen, M. Joshi, A. Shibata, N. Tsuji, Yielding behavior and its effect on uniform elongation in IF steel with various grain sizes, J. Mater. Sci. 49 (2014) 6536–6542.
[29] N. Tsuji, S. Ogata, H. Inui, I. Tanaka, K. Kishida, S. Gao, W. Mao, Y. Bai, R. Zheng, J. Du, Strategy for managing both high strength and large ductility in structural materials-sequential nucleation of different deformation modes based on a concept of plaston, Scr. Mater. 181 (2020) 35–42.
[30] E.O. Hall, The deformation and ageing of mild steel: III. Discussion of results, Proc. Phys. Soc. Lond. B 64 (1951) 747–753.
[31] N.J. Petch, The cleavage strength of polycrystals, J. Iron Steel Inst 174 (1953) 25–28.
[32] N. Ono, R. Nowak, S. Miura, Effect of deformation temperature on Hall-Petch relationship registered for polycrystalline magnesium, Mater. Lett. 58 (2004) 39–43.
[33] H. Somekawa, T. Mukai, Hall-Petch relation for deformation twinning in solid solution magnesium alloys, Mater. Sci. Eng. A 561 (2013) 378–385.
[34] D.A. Hughes, N. Hansen, Exploring the limit of dislocation based plasticity in nanostructured metals, Phys. Rev. Lett. 112 (2014) 135504.
[35] C.A. Schuh, T.G. Nieh, H. Iwasaki, The effect of solid solution W additions on the mechanical properties of nanocrystalline Ni, Acta Mater 51 (2003) 431–443.
[36] M.A. Meyers, A. Mishra, D.J. Benson, Mechanical properties of nanocrystalline materials, Prog. Mater. Sci. 51 (2006) 427–556.
[37] R. Zheng, T. Bhattacharjee, S. Gao, W. Gong, A. Shibata, T. Sasaki, K. Hono, N. Tsuji, Change of Deformation Mechanisms Leading to High Strength and Large Ductility in Mg-Zn-Zr-Ca Alloy with Fully Recrystallized Ultrafine Grained Microstructures, Sci Rep 9 (2019) 1–14.
[38] Z.R. Lin, A.H. Chokshi, T.G. Langdon, An investigation of grain boundary sliding in superplasticity at high elongations, J. Mater. Sci. 23 (1988) 2712–2722.
[39] D.B. Williams, C.B. Carter, Transmission Electron Microscopy: A textbook for materials science, Springer, 2009.
[40] R.L. Bell, T.G. Langdon, An investigation of grain-boundary sliding during creep, J. Mater. Sci. 2 (1967) 313–323.
[41] T. Kunimine, N. Takata, N. Tsuji, T. Fujii, M. Kato, S. Onaka, Temperature and strain rate dependence of flow stress in severely deformed copper by accumulative roll bonding, Mater. Trans. 50 (2009) 64–69.
[42] T. Kunimine, T. Fujii, S. Onaka, N. Tsuji, M. Kato, Effects of Si addition on mechanical properties of copper severely deformed by accumulative roll-bonding, J. Mater. Sci. 46 (2011) 4290–4295.
[43] R.B. Figueiredo, F.S. Poggiali, C.L. Silva, P.R. Cetlin, T.G. Langdon, The influence of grain size and strain rate on the mechanical behavior of pure magnesium, J. Mater. Sci. 51 (2016) 3013–3024.
[44] T.G. Nieh, J. Wadsworth, O.D. Sherby, Superplasticity in Metals and Ceramics, Cambridge University Press, 2005.
[45] X. Wang, L. Jiang, D. Zhang, T.J. Rupert, I.J. Beyerlein, S. Mahajan, E.J. Lavernia, J.M. Schoenung, Revealing the deformation mechanisms for room-temperature compressive superplasticity in nanocrystalline magnesium, Materialia 11 (2020) 100731.
[46] G.W. Groves, A. Kelly, Change of shape due to dislocation climb, Philos. Mag. 19 (1969) 977–986.
[47] J.P. Hirth, J. Lothe, Theory of Dislocations, Wiley, 1982.
[48] W.B. Hutchinson, M.R. Barnett, Effective values of critical resolved shear stress for slip in polycrystalline magnesium and other hcp metals, Scr. Mater. 63 (2010) 737–740.
[49] R.W. Armstrong, 60 years of Hall-Petch: past to present nano-scale connections, Mater. Trans. 55 (2014) 2–12.
[50] Z.C. Cordero, B.E. Knight, C.A. Schuh, Six decades of the Hall-Petch effect-a survey of grain-size strengthening studies on pure metals, Int. Mater. Rev. 61 (2016) 495–512.
[51] K.S. Kumar, H. Van Swygenhoven, S. Suresh, Mechanical behavior of nanocrystalline metals and alloys, Acta Mater 51 (2003) 5743–5774.
[52] D.E. Spearot, K.I. Jacob, D.L. McDowell, Dislocation nucleation from bicrystal interfaces with dissociated structure, Int. J. Plast. 23 (2007) 143–160.
[53] S. Ogata, J. Li, N. Hirosaki, Y. Shibutani, S. Yip, Ideal shear strain of metals and ceramics, Phys. Rev. B 70 (2004) 104104.
[54] L.J. Slutsky, C.W. Garland, Elastic constants of magnesium from 4.2 K to 300 K, Phy. Rev. 107 (1957) 972–976.
[55] J.C.M. Li, G.C.T. Liu, Circular dislocation pile-ups: I. Strength of ultra-fine polycrystalline aggregates, Philos. Mag. 15 (1967) 1059–1063.
[56] M.V. Klassen-Neklyudova, Mechanical twinning of crystals, Springer Science & Business Media, 2012.
[57] A. Ishii, J. Li, S. Ogata, Shuffling-controlled *versus* strain-controlled deformation twinning: the case for Mg, Int. J. Plast. 82 (2016) 32–43.

[58] A. Chapuis, J.H. Driver, Temperature dependency of slip and twinning in plane strain compressed magnesium single crystals, Acta Mater 59 (2011) 1986–1994.
[59] S. Yip, Nanocrystals: the strongest size, Nature 391 (1998) 532–533.
[60] A.S. Argon, S. Yip, The strongest size, Philos. Mag. Lett. 86 (2006) 713–720.
[61] I.G. Crossland, R.B. Jones, Grain boundary diffusion creep in magnesium, Met. Sci. 11 (1977) 504–508.
[62] H.J. Frost, M.F. Ashby, Deformation-mechanism maps: the plasticity and creep of metals and ceramics, Pergamon-Press, Oxford, 1982.
[63] R. Zheng, H. Somekawa, N. Tsuji, Effect of trace Zn addition on the mechanical properties of bulk ultrafine-grained Mg, unpublished.
[64] D.A. Basha, R. Sahara, H. Somekawa, J.M. Rosalie, A. Singh, K. Tsuchiya, Interfacial segregation induced by severe plastic deformation in a Mg-Zn-Y alloy, Scr. Mater. 124 (2016) 169–173.
[65] X. Zhou, X. Li, K. Lu, Size Dependence of Grain Boundary Migration in Metals under Mechanical Loading, Phys. Rev. Lett. 122 (2019) 126101.
[66] H. Somekawa, A. Singh, T. Mukai, T. Inoue, Effect of alloying elements on room temperature tensile ductility in magnesium alloys, Philos. Mag. 96 (2016) 2671–2685.
[67] H. Somekawa, A. Kinoshita, K. Washio, A. Kato, Enhancement of room temperature stretch formability via grain boundary sliding in magnesium alloy, Mater. Sci. Eng. A 676 (2016) 427–433.
[68] H. Somekawa, A. Singh, Superior room temperature ductility of magnesium dilute binary alloy via grain boundary sliding, Scr. Mater. 150 (2018) 26–30.